Aerospace Science and Technology 114 (2021) 106750

Contents lists available at ScienceDirect

Aerospace Science and Technology

www.elsevier.com/locate/aescte

Finite-time distributed hierarchical control for satellite cluster with collision avoidance

Siyuan Li [a], Chuang Liu [a,b,*], Zhaowei Sun [a]

[a] Research Center of Satellite Technology, Harbin Institute of Technology, Harbin 150001, China
[b] School of Astronautics, Northwestern Polytechnical University, Xi'an 710072, China

ARTICLE INFO

Article history:
Received 3 August 2020
Received in revised form 3 January 2021
Accepted 12 April 2021
Available online 22 April 2021
Communicated by Chaoyong Li

Keywords:
Satellite cluster
Hierarchical control
Collision avoidance
Multiple disturbances
Input constraints

ABSTRACT

In this paper, a novel distributed hierarchical control method for small satellites with multiple disturbances and input constraints is investigated by combining formation flying and satellite cluster. First, a finite-time convergent extended state observer (FTCESO) is developed to estimate the external disturbance with high precision, and a non-singular fast terminal sliding mode controller (NFTSMC) is proposed to maintain the specific configuration of leader-satellites and the finite time convergence is theoretically proved. Then, an improved artificial potential field method with collision avoidance and damping characteristics is proposed for the follower-satellite, so that the follower-satellite can keep a collision-avoidance relative distance from corresponding leader-satellite with the desired communication range. Finally, numerical simulations are performed to demonstrate the effectiveness of the proposed method.

1. Introduction

Recent years we have witnessed rapid development of small satellites which can use space network to fully realize the complex performance of traditional large satellites. In addition, small satellites can greatly reduce the costs and risks borne by large satellites, and significantly increase the flexibility and robustness of the system [1–3]. A distributed satellite system (DSS) may include multiple satellites distributed in one or more orbits according to certain requirements and cooperating with each other to perform a space flight mission, e.g. observation, communication, reconnaissance, navigation. It should be mentioned that constellations, formation flying, and satellite cluster all belong to distributed satellite systems [4]. Satellites in the constellation fly in multiple orbits and can effectively increase ground coverage and shorten revisit period, e.g. GPS, GLONASS, Galileo, Beidou [5]. Unlike constellation and formation flying, satellite cluster need no precise geometric structures [6]. The geometry of the relative orbits is loose, and only the maximum and minimum distances between satellites should be maintained during the entire mission life [7].

The main challenge of formation flying and satellite cluster is the complex dynamic coupling between satellites and the environment. If small satellites are launched into low-Earth orbit, they will be affected by environmental disturbances, e.g. atmospheric drag, solar pressure, and J_2 perturbation [8]. Without active control, these disturbances will cause rapid satellites drift. Since satellite formation flight needs to maintain a fixed spatial configuration, so that a compensation for uncertain disturbances is essential. The extended state observer (ESO)-based active disturbance rejection control (ADRC) provides a novel idea for solving the above problem. The states of system and uncertain disturbances can be estimated quickly without accurate measurement [9,10]. However, the linear ESO with high gain characteristics has an undesirable peak phenomenon and can only asymptotically converge in an infinite time interval [11]. In order to solve these problems, a finite-time convergent extended state observer (FTCESO) was presented in [12] and [13], which can achieve finite-time convergence without peak phenomenon. In addition, sliding mode control is an effective robust control method for uncertain systems because of its remarkable robustness and fast response to external disturbances and parameter uncertainties, which has been widely used in formation flying control [14–16]. Terminal sliding mode control (TSMC) can solve the shortcomings of linear sliding mode control that cannot converge in finite time, but singularity also occurs [17]. When the system state is far from the equilibrium point, the

* Corresponding author at: Research Center of Satellite Technology, Harbin Institute of Technology, Harbin 150001, China; School of Astronautics, Northwestern Polytechnical University, Xi'an 710072, China.
E-mail address: liuchuangforever@msn.com (C. Liu).

https://doi.org/10.1016/j.ast.2021.106750
1270-9638/

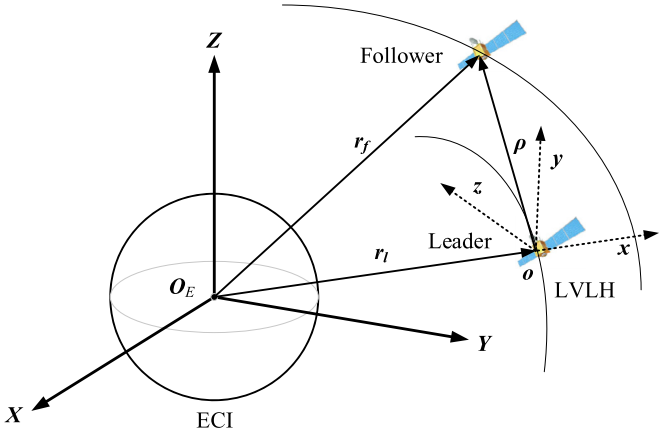

Fig. 1. Satellite docking system.

convergence speed of TSMC is non-ideal, even lower than linear sliding mode control [18]. Thus, a non-singular fast terminal sliding mode controller (NFTSMC) is proposed in [19]. In recent years, there have been many studies based on ESO and NFTSMC, but few results have been applied in satellite formation flying and satellite cluster [20–22].

Compared with satellite formation flying, satellite cluster does not require a specific spatial configuration. The relative distance between satellites during the flight should be maintained between the maximum and minimum distance, where the maximum distance is determined by the communication limit distance, and the minimum distance is to ensure collision avoidance between satellites. Active control is indispensable due to the influence of space disturbances, even if satellite cluster has relatively loose constraints on the relative distance. A feedback control method has been used in [7] to make the average orbit element of the satellites in the cluster reach the set reference value to achieve long-term relative distance maintenance. Combined with the on-off cyclic control, a fuel optimal control law was proposed under uncertain thrust conditions to keep the satellites within given distance bounds for the entire mission lifetime [23]. In addition, there is much literature investigating control methods for satellite cluster [24–28]. The key of these control methods is to control the mean semi-major axis, eccentricity and orbit inclination of the satellites to meet J_2 invariant condition, so that the cluster satellites won't drift under the condition of J_2 perturbation. However, when other disturbances, e.g. atmospheric drag and solar pressure, are taken into account, the J_2 invariant condition is no longer applicable, which poses a great challenge to derive the bounded condition of the relative motion of the satellite under complex space disturbance [29].

The artificial potential field method is a virtual force method that was originally used for the control of mobile robots [30]. In the control strategy using artificial potential field, the target point produces attractive force to the mobile robot, and the obstacle produces repulsive force. Then, the motion of the mobile robot can be generated by finding the resultant force. Finally, the resultant force is calculated to control the flight of the mobile robot. In recent years, the artificial potential field method is often applied to collision avoidance and path planning of robots, spacecraft, and multi-agents [31,32]. Because the artificial potential field method can artificially set the motion 'forbidden zone', and the mathematical description is simple, it is very suitable for satellite cluster control.

In a space mission including multiple small satellites, there may be a certain number of small satellites with a fixed space configuration. However, some small satellites only need to have communication with their associated satellites and keep a safe flight distance. Thus, the satellite cluster can be divided into different levels combining formation flying and satellite cluster to meet the requirements of complex space missions. To our knowledge, little research has explicitly focused on the aforementioned issues. This paper documents several key contributions made to the complex multi-satellite mission. Firstly, multiple small satellites are divided into leader layer and follower layer, and a hierarchical control strategy combining formation flying and satellite cluster is investigated. Secondly, the synchronous control of the leader layer with various spatial disturbances and input constraints is achieved by using FTCESO and NFTSMC. Finally, an improved artificial potential field method including dynamic obstacle avoidance and damping characteristics is proposed for the follower layer, which makes the followers collision-avoidance flight and ensure communication, and also support external satellites to join the cluster at any time.

The rest of this paper is organized as follows. Section 2 describes the dynamics model of satellite rendezvous, graph theory and some related lemmas. In Section 3, a synchronization controller based on FTCESO and NFTSMC is developed for the leader layer, and corresponding stability analysis is performed via a Lyapunov approach. Furthermore, an improved artificial potential field method is designed for the follower layer. Section 4 demonstrates the effectiveness of the controller by numerical examples. Some conclusions are drawn in the final section.

2. Problem formulation

2.1. Dynamics model of relative motion of satellite cluster

As shown in Fig. 1, the Earth-centered inertial (ECI) frame and local-vertical local-horizontal (LVLH) frame are commonly used to describe the relative motion between satellites. According to Newton second law, the relative dynamics equation between the follower and leader satellites is expressed by the following equation:

$$\begin{cases} \dfrac{d^2\mathbf{r}_f}{dt} = -\dfrac{\mu \mathbf{r}_f}{r_f^3} + \mathbf{f}_f + \mathbf{u}_f \\ \dfrac{d^2\mathbf{r}_l}{dt} = -\dfrac{\mu \mathbf{r}_l}{r_l^3} + \mathbf{f}_l + \mathbf{u}_l \end{cases} \tag{1}$$

where $\mathbf{r}_l$ and $\mathbf{r}_f$ are the position vectors of the leader and follower satellites in ECI frame; $\mathbf{f}_l$ and $\mathbf{f}_f$ are the acceleration vectors of perturbation forces exerted on leader and follower satellites except for the gravity of the Earth; $\mathbf{u}_l$ and $\mathbf{u}_f$ are the acceleration vectors of thrust. The model in [30] expresses the components of relative motion in LVLH frame as shown in Eq. (2).

$$\begin{cases} \ddot{x} - \dot{n}_0 y - {n_0}^2 x - 2n_0 \dot{y} = -\dfrac{\mu (R+x)}{\left[(R+x)^2 + y^2 + z^2\right]^{\frac{3}{2}}} + \dfrac{\mu}{R^2} + \dfrac{u_x}{m_f} + F_x \\ \ddot{y} + \dot{n}_0 x - {n_0}^2 y + 2n_0 \dot{x} = -\dfrac{\mu y}{\left[(R+x)^2 + y^2 + z^2\right]^{\frac{3}{2}}} + \dfrac{u_y}{m_f} + F_y \\ \ddot{z} = -\dfrac{\mu z}{\left[(R+x)^2 + y^2 + z^2\right]^{\frac{3}{2}}} + \dfrac{u_z}{m_f} + F_z \end{cases} \tag{2}$$

where n_0 is the orbital frequency of leader satellite, R represents the norm of position vector from the center of Earth to leader satellite, μ is the gravitation constant, m_f is the mass of the follower satellite, u_x, u_y, u_z represent the thrust force of the thruster in the direction of three coordinate axes, and F_x, F_y, F_z represent the disturbing force in the direction of three coordinate axes. Define $\rho = [x, y, z]$, $\dot{\rho} = [\dot{x}, \dot{y}, \dot{z}]$, $u_f = [u_x, u_y, u_z]$, and Eq. (2) can be written as Eq. (3).

$$m_f \ddot{\rho} + m_f N(n_0)\, \dot{\rho} + m_f M(\rho, n_0, R) = F_d + u_f \tag{3}$$

where

$$N(n_0) = \begin{bmatrix} 0 & -2n_0 & 0 \\ 2n_0 & 0 & 0 \\ 0 & 0 & 0 \end{bmatrix}, \qquad M(\rho, n_0, R) = \begin{bmatrix} -\dot{n}_0 y - {n_0}^2 x + \frac{\mu(R+x)}{\left[(R+x)^2+y^2+z^2\right]^{\frac{3}{2}}} - \frac{\mu}{R^2} \\ \dot{n}_0 x - {n_0}^2 y + \frac{\mu y}{\left[(R+x)^2+y^2+z^2\right]^{\frac{3}{2}}} \\ \frac{\mu z}{\left[(R+x)^2+y^2+z^2\right]^{\frac{3}{2}}} \end{bmatrix}$$

2.2. Space perturbations

On-orbit satellite will be affected by space perturbations, where J_2 perturbation and atmospheric drag have the greatest impact on relative motion of satellites in low Earth orbit.

The J_2 perturbation is caused by the uneven density distribution of the Earth, which is not a regular sphere. The gravitational potential function of the Earth is expressed by Eq. (4).

$$U = \frac{G_M}{R}\left\{1 - \sum_{n=2}^{\infty}\left(\frac{R_e}{R}\right)^2\left[J_n P_n \sin^2\delta - \sum_{m=1}^{n} J_{nm} P_{nm} \sin\delta \cos m(\lambda - \lambda_{nm})\right]\right\} \tag{4}$$

where G_M is the gravitational constant; R_e is the average radius of the Earth; R is the geocentric distance; λ and δ is the longitude and latitude; P_n and P_{nm} is the Legendre polynomials; J_n is the coefficient of the zonal harmonic, J_{nm} and λ_{nm} are the coefficients of the tesseral and sectorial harmonics. The magnitude of J_2 perturbation is much larger than that of other non-spherical perturbations for a low-Earth-orbit satellite. After derivation calculus to gravitational potential function, the acceleration component form of the near-Earth satellite under J_2 perturbation can be obtained as Eq. (5).

$$\begin{cases} \dfrac{d^2x}{dt^2} = -\dfrac{G_M x}{R^3}\left[\dfrac{3}{2}J_2\left(\dfrac{R_e}{R}\right)^2\left(1 - 5\dfrac{z^2}{R^2}\right)\right] \\ \dfrac{d^2y}{dt^2} = -\dfrac{G_M y}{R^3}\left[\dfrac{3}{2}J_2\left(\dfrac{R_e}{R}\right)^2\left(1 - 5\dfrac{z^2}{R^2}\right)\right] \\ \dfrac{d^2z}{dt^2} = -\dfrac{G_M z}{R^3}\left[\dfrac{3}{2}J_2\left(\dfrac{R_e}{R}\right)^2\left(3 - 5\dfrac{z^2}{R^2}\right)\right] \end{cases} \tag{5}$$

where x, y and z are the components of position vector. The term $J_2 = 0.0010826$ denotes the second-order zonal harmonic coefficient.

In addition to the J_2 perturbation, atmospheric drag is another important perturbation force that affects low-Earth orbit satellites and the acceleration can express as Eq. (6), i.e.

$$a = -\frac{1}{2}\frac{C_D A}{m}\varphi v_{rel} \boldsymbol{v_{rel}} \tag{6}$$

where C_D is the drag coefficient, A is the cross-sectional area, m is the mass of the satellite, φ is the atmospheric density, $\boldsymbol{v_{rel}}$ is the speed vector of the satellite relative to the atmosphere which can be obtained by Eq. (7).

$$\boldsymbol{v_{rel}} = \frac{d\boldsymbol{R}}{dt} - \boldsymbol{\omega} \times \boldsymbol{R} \tag{7}$$

where $\boldsymbol{R}$ denotes the satellite position vector, $\boldsymbol{\omega}$ is the angular velocity of the Earth's rotation and the direction is along the positive direction of the Z axis. In addition, this paper uses an exponential atmospheric density model, i.e.

$$\varphi = \varphi_0 e^{-(R-R_0)/H} \tag{8}$$

where $H = H_0 + \mu_0 (R - R_0)$, φ_0 is the atmospheric density at the reference point, R_0 is the geocentric distance of reference point, H is the scale height and H_0 is the scale height at the reference point, μ_0 is a constant of about 0.2 whose maximum will not exceed 0.4.

2.3. Graph theory

In general, the information exchange between satellites can be modeled with undirected graphs. Let $G = (V, E)$ be an undirected graph with N nodes and the node set is written as $V = \{v_1, v_2, \cdots, v_N\}$. Its edge is $E = \{e_1, e_2, \cdots, e_M\}$ representing the information flow between nodes. If e is the edge connecting nodes v_i and v_j in the graph $G = (V, E)$, then v_i and v_j are adjacent to each other. a_{ij} is used to represent the connection relationship between nodes v_i and v_j. Then $a_{ij} = 1$ if there is an edge between nodes v_i and v_j; otherwise, $a_{ij} = 0$. The matrix $A(G) = \left(a_{ij}\right)_{n\times n}$ is called the adjacency matrix which is obviously a symmetric matrix and a non-negative matrix.

Define the matrix $L_n = \left(l_{ij}\right)_{n\times n}$ that $l_{ij} = \sum_{j=1, j\neq i}^{n} a_{ij}, l_{ij} = -a_{ij}, i \neq j$. It is obvious that $l_{ij} \leq 0, i \neq j$ and $\sum_{j=1}^{p} l_{ij} = 0, i = 1, 2, \cdots, n$. We called L_n as Laplacian matrix. L_n of a undirected graph is symmetric and L_n is a positive semi-definite matrix if the undirected graph is connected.

2.4. Some lemmas

Lemma 1. *[19]: Suppose that there exists a continuous differential positive definite function $V(t)$, and $\alpha > 0$, $\beta > 0$, $0 < r < 1$ are real numbers. If $V(t)$ satisfies the differential inequality Eq. (9). Then, $V(t)$ will converge to the equilibrium point in a finite time t_f, where t_f can be obtained by Eq. (10).*

$$\dot{V} + \alpha V + \beta V^r \leq 0 \quad \forall > t_0 \tag{9}$$

$$t_f \leq t_0 + \frac{1}{\alpha (1-r)} \ln \frac{\alpha V^{1-r}(x_0) + \beta}{\beta} \tag{10}$$

Lemma 2. *[19]: If the matrix R is a positive definite symmetric matrix, and there are positive numbers c_1 and c_2, then the matrix can have the relationship as in Eq. (11).*

$$c_2 \|x\|^2 \leq x^T \mathrm{R} x \leq c_1 \|x\|^2 \quad \forall x \in \mathbf{R}^3 \tag{11}$$

3. Controller design

In this section, the hierarchical control of distributed satellites is discussed. Due to space mission requirements, the satellites are divided into two layers. Some satellites need to have a specific spatial configuration which are the first layer called the leader layer. Each satellite in the leader layer need some satellites to provide services, and these satellites only need to maintain a communication distance with their leader satellite. In this case, these satellites denoting follower layer are called the second layer.

3.1. Synchronization control law for the leader layer

The leader layer contains a virtual reference satellite and N real satellites which can obtain position and speed information between each other through wireless communication. Suppose that these satellites have the same mass m_f. In the LVLH frame, the desired position of the i-th satellite relative to the virtual reference satellite is $\rho_{id} = [x_{id}, y_{id}, z_{id}]$, the desired speed is $\dot{\rho}_{id} = [\dot{x}_{id}, \dot{y}_{id}, \dot{z}_{id}]$. The position tracking error of the $i-$th satellite is defined as $e_{i1} = \rho_i - \rho_{id}$, and the corresponding speed tracking error is $e_{i2} = \dot{\rho}_i - \dot{\rho}_{id}$. According to Eq. (3), the relative motion error model of satellites can be obtained as Eq. (12).

$$\begin{cases} \dot{e}_{i1} = e_{i2} \\ \dot{e}_{i2} = g(\rho_i, \dot{\rho}_i, \ddot{\rho}_i) + \dfrac{1}{m_f} F_{id} + \dfrac{1}{m_f} u_i \end{cases} \tag{12}$$

where $g(\rho_i, \dot{\rho}_i, \ddot{\rho}_i)$ is a nonlinear function of Eq. (13), F_{id} is the space disturbance including J_2 perturbation and atmospheric drag, u_i is the control force of the i-th satellite.

$$g(\rho_i, \dot{\rho}_i, \ddot{\rho}_i) = \begin{bmatrix} \dot{n}_0 y_i + {n_0}^2 x_i + 2n_0 \dot{y}_i - \dfrac{\mu (R + x_i)}{\left[(R + x_i)^2 + {y_i}^2 + {z_i}^2\right]^{\frac{3}{2}}} + \dfrac{\mu}{R^2} - \ddot{x}_{id} \\ -\dot{n}_0 x_i + {n_0}^2 y_i - 2n_0 \dot{x}_i - \dfrac{\mu y_i}{\left[(R + x_i)^2 + {y_i}^2 + {z_i}^2\right]^{\frac{3}{2}}} - \ddot{y}_{id} \\ -\dfrac{\mu z_i}{\left[(R + x_i)^2 + {y_i}^2 + {z_i}^2\right]^{\frac{3}{2}}} - \ddot{z}_{id} \end{bmatrix} \tag{13}$$

It is worth noting that the perturbation model is calculated in the ECI frame, and it can be transformed into the LVLH frame through coordinate transformation. Using the orbital elements of the virtual satellite, the transformation matrix of the geocentric inertial coordinate system to the LVLH coordinate system can be obtained as

$$F_{idLVLH} = C_z(\omega + \theta) C_x(i) C_z(\Omega) F_{idECI} \tag{14}$$

where Ω is the longitude ascending node, i is the orbit inclination, ω is the argument of perigee, θ is the true anomaly, and

$$C_z(\omega + \theta) = \begin{bmatrix} \cos(\omega + \theta) & \sin(\omega + \theta) & 0 \\ -\sin(\omega + \theta) & \cos(\omega + \theta) & 0 \\ 0 & 0 & 1 \end{bmatrix}, \quad C_x(i) = \begin{bmatrix} 1 & 0 & 0 \\ 0 & \cos i & \sin i \\ 0 & -\sin i & \cos i \end{bmatrix}, \quad C_z(\Omega) = \begin{bmatrix} \cos\Omega & \sin\Omega & 0 \\ -\sin\Omega & \cos\Omega & 0 \\ 0 & 0 & 1 \end{bmatrix}$$

Next, the FTCESO will be designed. According to Eq. (12), let $e_{i1} = x_{i1}$, $e_{i2} = x_{i2}$, the relative motion error of the satellite in leader layer can be written as

$$\begin{cases} \dot{x}_{i1} = x_{i2} \\ \dot{x}_{i2} = x_{i3} + \dfrac{1}{m_f} u_i \\ \dot{x}_{i3} = \dot{L}(t) \end{cases} \tag{15}$$

where $L(t) = g(\rho_i, \dot{\rho}_i, \ddot{\rho}_i) + \frac{1}{m_f} F_{id}$. The variables ρ_i, $\dot{\rho}_i$ and $\ddot{\rho}_i$ are continuous and bounded in practice and the denominators in $\frac{d}{dt} g(\rho_i, \dot{\rho}_i, \ddot{\rho}_i)$ are not zero. Otherwise the F_{id} is continuous and slowly-varying. So we suppose $\left|\dot{L}(t)\right| \le U_f$.

It is obvious that the system is observable, and then a FTCESO is constructed as [12]

$$\begin{cases} e_i = x_{i1} - z_{i1} \\ \dot{z}_{i1} = z_{i2} + k_1 sig^{(\kappa+1)/2} e_i \\ \dot{z}_{i2} = z_{i3} + k_2 sig^{(\kappa+1)/2} e_i + \dfrac{1}{m_f} u_i \\ \dot{z}_{i3} = k_3 sig^{\kappa} e_i \end{cases} \tag{16}$$

where, z_{i1}, z_{i2} and z_{i3} are the estimated values of x_{i1}, x_{i2} and x_{i3}, $\kappa \in (0, 1)$, k_1, k_2 and k_3 are the observer gains, e_i is the system output error, and $sig^{\kappa}(\cdot) = \mathrm{sgn}(\cdot)|\cdot|^{\kappa}$. In addition, the observation error of FTCESO can be defined as $\varepsilon_i = x_i - z_i$, $i \in \{1, 2, 3\}$ with its derivative as

$$\begin{cases} \dot{\varepsilon}_1 = \varepsilon_2 - k_1 sig^{(\kappa+1)/2}(\varepsilon_1) \\ \dot{\varepsilon}_2 = \varepsilon_3 - k_2 sig^{(\kappa+1)/2}(\varepsilon_1) \\ \dot{\varepsilon}_3 = -\dot{x}_3 - k_3 sig^{\kappa}(\varepsilon_1) \end{cases} \tag{17}$$

Lemma 3. *[12]: With the assumption $\left|\dot{L}(t)\right| \le U_f$ satisfied, there exist constants $k_1 > 0$, $k_2 > 0$, $k_3 > 0$, $0 < \kappa < 1$, $t_f > 0$ make the FTCESO (16) that*

$$\|\boldsymbol{\varepsilon}\| \le \frac{l U_f}{\sigma_{\min}\{D\} \cdot \sigma_{\min}\{E\}} = \varepsilon_f, \forall t > t_f \tag{18}$$

with $t_f \le \frac{2(\alpha+\beta)}{\alpha\beta} (\lambda_{\max}\{E\} V(\boldsymbol{\varepsilon}_0))^{1/2}$, where, $\boldsymbol{\varepsilon} = [\, sig^{(\kappa+1)/2}(\varepsilon_1), \quad \varepsilon_2, \quad \varepsilon_3 \,]^T$, $\boldsymbol{\varepsilon}_0$ is the initial observation error, $\sigma_{\min}\{\cdot\}$ is the smallest singular value of the matrix, and the maximum eigenvalue of the matrix is expressed as $\lambda_{\max}$. Furthermore, one has

$$\begin{aligned} l &= \sqrt{{k_3}^2 + 4} \\ D &= \begin{bmatrix} k_1 & -1 & 0 \\ k_2 & 0 & -1 \\ k_3 & 0 & 0 \end{bmatrix} \\ E &= \begin{bmatrix} 2k_1/(\kappa + 1) + k_2^2 + k_3^2 & -k_2 & -k_3 \\ -k_2 & 2 & 0 \\ -k_3 & 0 & 2 \end{bmatrix} \end{aligned} \tag{19}$$

The expressions of α, β, $V(\cdot)$ are

$$\begin{aligned} \alpha &= (\kappa + 1)\sigma_{\min}\{D\}\sigma_{\min}\{E\} - 2lU_f \\ \beta &= 2\varepsilon_f \sigma_{\min}\{D\}\sigma_{\min}\{E\} - 2lU_f \\ V(\varepsilon) &= \varepsilon^T E \varepsilon \end{aligned} \tag{20}$$

Therefore, by choosing appropriate values of k_1, k_2 and k_3, the observation error $\boldsymbol{\varepsilon}$ can converge to a small value within a finite time t_f.

For system (12), define the non-singular fast terminal sliding mode function as

$$s_i = x_{i2} + a x_{i1} + b x_{i1}^{q/p} \tag{21}$$

where a and b are constants, $a, b > 0$, q and p are odd, $q < p < 2q$.

Based on the satellite relative motion error model (12), FTCESO (16) and NFTSMC (21), the satellite synchronization controller is designed as

$$\begin{cases} u_i = u_{i1} + u_{i2} + u_{i3} \\ u_{i1} = -m_f \left(z_{i3} + a x_{i2} + \dfrac{bq}{p} x_{i1}^{(q-p)/p} \right) \\ u_{i2} = -m_f \left(K_{i1} s_i + K_{i2} s_i^{\upsilon} \right) \\ u_{i3} = -m_f \sum\limits_{j=1}^{n} a_{ij} \left(s_i - s_j \right) \end{cases} \tag{22}$$

where a_{ij} is the element in the row i and column j of the adjacency matrix A between satellites in leader layer, K_{i1} and K_{i2} are the control gains, u_{i1} is used to observe and compensate for the nonlinear term and space disturbances. The role of u_{i2} is to make the states of satellites reach the terminal sliding mode, and u_{i3} is the synchronization control item, which can make the satellites reach a stable state at the same time.

Theorem 1. *Considering the satellite formation control of leader layer described by the control law (22), if the approximation error of the FTCESO is bounded, then s_i is uniformly ultimately bounded.*

Proof. Choose a Lyapunov function candidate as

$$V = \sum_{i=1}^{n} V_i = \frac{1}{2} \sum_{i=1}^{n} s_i^T s_i \tag{23}$$

The time derivative of V is given by

$$\dot{V} = \sum_{i=1}^{n} \dot{V}_i = \sum_{i=1}^{n} s_i^T \dot{s}_i \tag{24}$$

Substituting Eqs. (12), (16), (21) and (22) into Eq. (24) yields the following expression, i.e.

$$\begin{aligned} \dot{V} &= \sum_{i=1}^{n} s_i^T \left(a x_{i2} + \frac{bq}{p} x_{i1}^{(q-p)/p} x_{i2} + \dot{x}_{i2} \right) \\ &= \sum_{i=1}^{n} s_i^T \left(a x_{i2} + \frac{bq}{p} x_{i1}^{(q-p)/p} x_{i2} + g\left(\rho_i, \dot{\rho}_i, \ddot{\rho}_i\right) + \frac{1}{m_f} F_{id} + \frac{1}{m_f} u_i \right) \\ &= \sum_{i=1}^{n} s_i^T \left(a x_{i2} + \frac{bq}{p} x_{i1}^{(q-p)/p} x_{i2} + g\left(\rho_i, \dot{\rho}_i, \ddot{\rho}_i\right) + \frac{1}{m_f} F_{id} - z_{i3} - a x_{i2} - \frac{bq}{p} x_{i1}^{(q-p)/p} x_{i2} \right. \\ &\quad \left. - \left(K_{i1} s_i + K_{i2} s_i^{\upsilon} \right) - \sum_{j=1}^{n} a_{ij} \left(s_i - s_j \right) \right) \end{aligned} \tag{25}$$

Let

$$\Delta_i = g\left(\rho_i, \dot{\rho}_i, \ddot{\rho}_i\right) + \frac{1}{m_f} F_{id} - z_{i3} \tag{26}$$

Define $\Delta_{\max} \geq \Delta_i$, then one has

$$\begin{aligned} \dot{V} &= \sum_{i=1}^{n} s_i^T \left(- \left(K_{i1} s_i + K_{i2} s_i^{\upsilon} \right) - \sum_{j=1}^{n} a_{ij} \left(s_i - s_j \right) + \Delta_{\max} \right) \\ &= - \sum_{i=1}^{n} s_i^T \left(K_{i1} s_i + K_{i2} s_i^{\upsilon} \right) - \sum_{i=1}^{n} s_i^T \sum_{j=1}^{n} a_{ij} \left(s_i - s_j \right) + \sum_{i=1}^{n} s_i^T \Delta_{\max} \end{aligned} \tag{27}$$

For

$$\begin{cases} -\sum_{i=1}^{n} {s_i}^T \sum_{j=1}^{n} a_{ij}\left(s_i - s_j\right) = -SL_nS^T \\ {s_i}^T \Delta_{\max} \le \frac{1}{2}{s_i}^T s_i + \frac{1}{2}\Delta_{\max}^2 \end{cases} \tag{28}$$

where $S = [s_1, s_2, \cdots, s_n]$ and L_n is the Laplacian matrix that corresponds to adjacency matrix of $A(G) = \left(a_{ij}\right)_{n\times n}$. For $A(G) = \left(a_{ij}\right)_{n\times n}$ is connected, the L_n is positive semi-definite. Therefore, $-\sum_{i=1}^{n} {s_i}^T \sum_{j=1}^{n} a_{ij}\left(s_i - s_j\right) \le 0$ and Eq. (27) reduces to

$$\begin{aligned} \dot{V} &\le -\sum_{i=1}^{n} {s_i}^T \left(K_{i1}s_i + K_{i2}{s_i}^{\upsilon}\right) + \sum_{i=1}^{n} {s_i}^T \Delta_{\max} \\ &\le -\sum_{i=1}^{n} {s_i}^T K_{i1}s_i - \sum_{i=1}^{n} {s_i}^T K_{i2}{s_i}^{\upsilon} + \frac{1}{2}{s_i}^T s_i + \frac{1}{2}\Delta_{\max}^2 \\ &\le -\lambda_{\min}(K_{i1})\sum_{i=1}^{n} {s_i}^T s_i - \sum_{i=1}^{n} {s_i}^T K_{i2}{s_i}^{\upsilon} + \frac{1}{2}{s_i}^T s_i + \frac{1}{2}\Delta_{\max}^2 \end{aligned} \tag{29}$$

where $\lambda_{\min}(K_{i1})$ represents the minimum eigenvalue of the gain matrix K_{i1}. According to [5] and Lemma 2, the term $\sum_{i=1}^{n} {s_i}^T K_{i2}{s_i}^{\upsilon}$ can be calculated as

$$\sum_{i=1}^{n} {s_i}^T K_{i2}{s_i}^{\upsilon} \le -\lambda_{\min}(K_{i2})\left(2pb/r_1q\right)^{(\upsilon+1)/2}\left({s_i}^T s_i\right)^{(\upsilon+1)/2} \tag{30}$$

Then, one has

$$\dot{V} \le -\gamma_1 \sum_{i=1}^{n} V_i - \gamma_2 \sum_{i=1}^{n} V_i^{(\upsilon+1)/2} + \frac{1}{2}\Delta_{\max}^2 \tag{31}$$

where $\gamma_1 = \lambda_{\min}(K_{i1})\left(2pb/r_1q\right) - 1$ and $\gamma_2 = \lambda_{\min}(K_{i2})\left(2pb/r_1q\right)^{(\upsilon+1)/2}$.

According to Eq. (31), the following two situations can be expressed as

$$\dot{V} \le -\sum_{i=1}^{n}\left(\gamma_1 - \frac{\Delta_{\max}^2}{2V_i}\right)V_i - \gamma_2 \sum_{i=1}^{n} V_i^{(\upsilon+1)/2} \tag{32}$$

$$\dot{V} \le -\gamma_1 \sum_{i=1}^{n} V_i - \sum_{i=1}^{n}\left(\gamma_2 - \frac{\Delta_{\max}^2}{2V_i^{(\upsilon+1)/2}}\right)V_i^{(\upsilon+1)/2} \tag{33}$$

According to Lemma 1, when $\gamma_1 - \frac{\Delta_{\max}^2}{2V_i} > 0$ and $\gamma_2 - \frac{\Delta_{\max}^2}{2V_i^{(\upsilon+1)/2}} > 0$, the system can achieve finite-time stability, and the sliding mode function will converge to the following area

$$\|s_i\| \le \min\left\{\sqrt{\frac{r_1\Delta_{\max}^2}{2r_2\lambda_{\min}(K_{i1})}}, \sqrt{\frac{r_1}{r_2}\left(\frac{\Delta_{\max}^2}{2r_2\lambda_{\min}(K_{i2})}\right)^{2/(\upsilon+1)}}\right\} \tag{34}$$

3.2. Collision avoidance control based on improved artificial potential field method

Each satellite in the leader layer is followed by m follower satellites requiring no specific spatial configuration. The follower satellites flying around a leader satellite form a follower layer. The follower satellites only need to maintain a communication distance with the leader satellite, and ensure that there is no collision between any two satellites.

In the LVLH frame centered on the leader satellite, the relative position vector of the i-th follower satellite is $\rho_{fi} = \left[x_{fi}, y_{fi}, z_{fi}\right]$, and the relative velocity vector is $\dot{\rho}_{fi} = \left[\dot{x}_{fi}, \dot{y}_{fi}, \dot{z}_{fi}\right]$. Assume that the mass of the follower satellite is m_f, then the relative motion model is the same as Eq. (12).

As shown in Fig. 2, the communication range of the leader satellite is divided into six areas, which are called no-fly zone, strong repulsion zone, repulsion transition zone, free flight zone, attraction transition zone and strong attraction zone. The terms d, r_1, r_2, h, a_1 and a_2 are the boundary radii of the above areas. In addition, one can set the resistance zone in the area except the no-fly zone and free flight zone.

According to these zones and the requirement of collision avoidance, the controller of the satellite in follower layer can be designed as

$$u_{fi} = u_{fi1} + u_{fi2} + u_{fi3} + u_{fi4} + u_{fi5} \tag{35}$$

where u_{fi1} only acts on the space between d and r_2 from the leader satellite, and u_{fi2} only acts on the space between h and a_2. Both of them use an improved artificial potential field method with transition zone to ensure that the follower satellite can fly between the no-fly

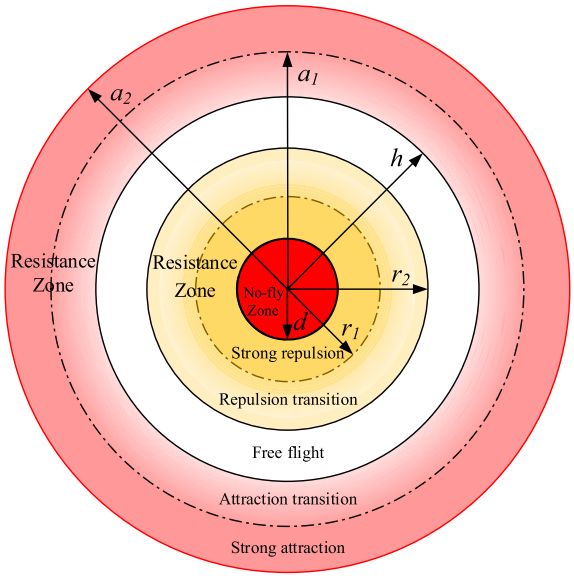

Fig. 2. Area division near the leader satellite.

zone boundary and the communication boundary of the leader satellite. Due to the transition zone, the satellites near the inner and outer borders will be under greater control, while the satellites near the free flight zone will be under less control. It keeps the satellites from being over-controlled and saves fuel. The expressions of u_{fi1} and u_{fi2} are

$$u_{fi1} = K_{fi1} b_i \eta_{fi1} \frac{\rho_{fi}}{\|\rho_{fi}\|_2}$$
$$\eta_{fi1} = \begin{cases} 1 & d < \|\rho_{fi}\|_2 < r_1 \\ \frac{1}{2}\left(1 + \cos\left(\pi \cdot \frac{\|\rho_{fi}\|_2 - r_1}{r_2 - r_1}\right)\right) & r_1 \le \|\rho_{fi}\|_2 \le r_2 \\ 0 & \text{other} \end{cases} \tag{36}$$

and

$$u_{fi2} = -K_{fi2} b_i \eta_{fi2} \frac{\rho_{fi}}{\|\rho_{fi}\|_2}$$
$$\eta_{fi2} = \begin{cases} 0 & \text{other} \\ \frac{1}{2}\left(1 - \cos\left(\pi \cdot \frac{\|\rho_{fi}\|_2 - h}{a_1 - h}\right)\right) & h \le \|\rho_{fi}\|_2 \le a_1 \\ 1 & a_1 < \|\rho_{fi}\|_2 \le a_2 \end{cases} \tag{37}$$

where K_{fi1} and K_{fi2} are the controller gains of u_{fi1} and u_{fi2}, b_i is a constant used to represent the connection between satellites. $b_i = 1$ if there exist direct or indirect communication between the i-th satellite and leader satellite, otherwise $b_i = 0$.

In this controller, u_{fi3} uses the repulsion function which is commonly used in artificial potential field method, with the expression as Eq. (38). The role of u_{fi3} is to ensure that the relative distance between the satellites in follower layer is always greater than the safety distance, so as to prevent the collisions between them.

$$u_{fi3} = -K_{fi3} \sum_{j=1}^{m} b_{ij} \eta_{fi3} \left(\rho_{fi} - \rho_{fj}\right)$$
$$\eta_{fi3} = \begin{cases} \left(\frac{1}{\|\rho_{fi} - \rho_{fj}\|_2} - \frac{1}{d}\right) \frac{1}{\|\rho_{fi} - \rho_{fj}\|_2^{\,2}} & \|\rho_{fi} - \rho_{fj}\|_2 - d \le d_i \\ 0 & \|\rho_{fi} - \rho_{fj}\|_2 - d > d_i \end{cases} \tag{38}$$

where d_i is the active area of the repulsion beyond the safe distance boundary, K_{fi3} the controller gain of u_{fi3}.

It is worth noting that the relative velocities of satellites may be very large during flight, and the control of u_{fi3} is only based on the relative position of the satellites. This method leads to unnecessary fuel consumption. Moreover, the safety distance between the satellites cannot be fully guaranteed in the case of constrained control. On this basis, an artificial potential field controller u_{fi4} based on the relative velocity is designed which play the role of dynamic avoidance. If the cosine of the angle between the relative velocity vectors

of two satellites and their relative position vector is less than zero, it means that the two satellites have a tendency to approach each other, and the controller u_{fi4} starts to work. The expression of u_{fi4} is

$$\begin{aligned} u_{fi4} &= -K_{fi4}\sum_{j=1}^{m} b_{ij}\eta_{fi4}\frac{\rho_{fi}-\rho_{fj}}{\left\|\rho_{fi}-\rho_{fj}\right\|_2} \\ \eta_{fi4} &= \begin{cases} \dfrac{\left(\rho_{fi}-\rho_{fj}\right)\cdot\left(\dot{\rho}_{fi}-\dot{\rho}_{fj}\right)}{\left\|\rho_{fi}-\rho_{fj}\right\|_2} & \left\|\rho_{fi}-\rho_{fj}\right\|_2 - d \le d_i, \quad \left(\rho_{fi}-\rho_{fj}\right)\cdot\left(\dot{\rho}_{fi}-\dot{\rho}_{fj}\right) \le 0 \\ 0 & \text{other} \end{cases} \end{aligned} \tag{39}$$

where K_{fi4} is the controller gain of u_{fi4}, b_{ij} is a constant used to represent the connection between satellites. $b_{ij}=1$ if there exist direct or indirect communication between the i-th satellite and the j-th satellite, otherwise $b_{ij}=0$.

When the demand for mission increases, the number of existing satellites is not enough to complete the mission, and other external satellites are often required to join the cluster. However, since the symmetric distribution of the repulsion and attraction zones, the external satellite cannot be controlled within the communication range of the leader satellite without proper deceleration. In addition, if the satellites in the follower layer are not decelerated, they will periodically and substantially fly between the repulsion and attraction zones, which will not only cause a large amount of fuel consumption, but even make the follower satellites fly out of the communication range of the leader under certain conditions. Therefore, the resistance potential field with smooth transition is designed, with its expression as

$$\begin{aligned} u_{fi5} &= -K_{fi5}b_i\eta_{fi5}\left\|\dot{\rho}_{fi}\right\|_2\dot{\rho}_{fi} \\ \eta_{fi5} &= \begin{cases} \dfrac{1}{2}\left(1+\cos\left(\pi\cdot\dfrac{\left\|\rho_{fi}\right\|_2-d}{r_2-d}\right)\right) & d<\left\|\rho_{fi}\right\|_2<r_2 \\ \dfrac{1}{2}\left(1-\cos\left(\pi\cdot\dfrac{\left\|\rho_{fi}\right\|_2-h}{a_2-h}\right)\right) & h\le\left\|\rho_{fi}\right\|_2\le a_2 \\ 0 & \text{other} \end{cases} \end{aligned} \tag{40}$$

where K_{fi5} is the controller gain of u_{fi5}.

Stability analysis is as follows:

Firstly, in controller u_{fi1} and u_{fi2}, we supposed that the initial position and velocity of the i-th follower satellite are ρ_{fi0} and $\dot{\rho}_{fi0}$. If the i-th follower satellite is moving close to the leader satellite, according to the Eq. (36), we can calculate the potential energy U_1 of the artificial potential field of u_{fi1} as

$$U_1 = \int_d^{\rho_{fi0}} \left(K_{fi1}b_i\eta_{fi1} - K_{fi2}b_i\eta_{fi2}\right)\frac{\rho}{\|\rho\|_2}\cdot\rho d\rho \tag{41}$$

If the i-th follower satellite is moving far away from the leader satellite, according to the Eq. (37), we can calculate the potential energy U_2 of the artificial potential field of u_{fi2} as

$$U_2 = \int_{\rho_{fi0}}^{a_2} \left(K_{fi2}b_i\eta_{fi2} - K_{fi1}b_i\eta_{fi1}\right)\frac{\rho}{\|\rho\|_2}\cdot\rho d\rho \tag{42}$$

And the kinetic energy E_i of the i-th follower satellite can calculate as

$$E_i = \frac{1}{2}\left\|\dot{\rho}_{fi0}\right\|^2 \tag{43}$$

Designing the control parameter K_{fi1} and K_{fi2} make $U_1 > E_i$ and $U_2 > E_i$, so that it can ensure the i-th follower satellite not only never enter the no-fly zone, but also never move beyond the communication distance of leader satellite. In conclusion, under the control of u_{fi1} and u_{fi2} the follower satellites are able to stabilize within the predetermined area.

Secondly, we know that the positions of the i-th and the j-th follower satellites are ρ_{fi} and ρ_{fj}. According to the Eq. (38) it is obvious that if $\left\|\rho_{fi}-\rho_{fj}\right\|_2\to 0$, $\left\|u_{fi3}\right\|_2\to\infty$. So the i-th and the j-th follower satellites are impossible to reach the distance of d. But consider the limit of thruster amplitude, the value of $\left\|u_{fi3}\right\|_2$ can not reach infinity. u_{fi4} is designed to cover this shortage. Suppose that the velocities of the i-th and the j-th follower satellites at the distance of $d+d_i$ are $\dot{\rho}_{fi}$ and $\dot{\rho}_{fj}$. Consider the worst case that the i-th and the j-th follower satellites are move towards each other. We can calculate the potential energy U_4 of the artificial potential field of u_{fi4} by Eq. (39)

$$U_4 = \int_d^{d_i} K_{fi4}b_i\eta_{fi4}\frac{\rho}{\|\rho\|_2}\cdot\rho d\rho \tag{44}$$

And E_i and E_j are the kinetic energy of i-th and the j-th follower satellites at the distance of $d+d_i$. Designing the control parameter K_{fi4} make $U_4 > E_i + E_j$ that

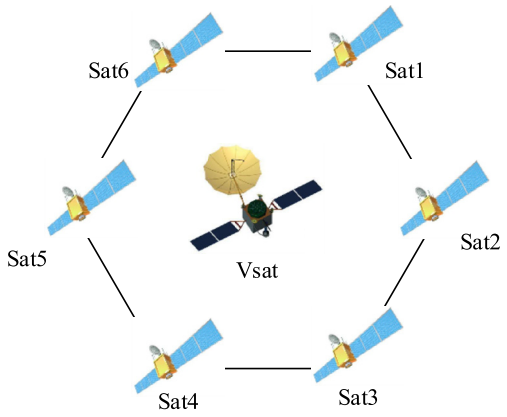

Fig. 3. Communication topology of the satellites in leader layer.

Table 1
Initial orbit elements of the virtual leader satellite.

a (km)	e	i (rad)	Ω (rad)	ω (rad)	f (rad)
6878.14	0.01	$\pi/3$	$\pi/6$	$\pi/4$	0

$$K_{fi4} > \frac{\left\|\dot{\rho}_{fi}\right\|^2 + \left\|\dot{\rho}_{fj}\right\|^2}{2\int_d^{d_i} K_{fi4} b_i \eta_{fi4} \frac{\rho}{\|\rho\|_2} \cdot \rho d\rho} \tag{45}$$

So it can ensure that the i-th and the j-th follower satellites will never move within the distance of d.

Finally, to make sure that other external satellites could join the cluster successfully we designed controller u_{fi5}. Suppose that the i-th follower satellite is the external satellite which plan to join the cluster and the velocity at the distance r_2 of it is $\dot{\rho}_{fi0}$. According to the Eq. (40), only consider the action of the controller u_{fi5}, we can calculate the time when the velocity reduces to zero

$$t = \int_0^{\dot{\rho}_{fi0}} \frac{1}{K_{fi5} b_i \eta_{fi5} \|\dot{\rho}\|_2 \dot{\rho}} d\dot{\rho} \tag{46}$$

Under the action of the controller u_{fi5}, it is obvious that the velocity of the satellite is decreasing all the time. Designing the control parameter K_{fi5} make $\dot{\rho}_{fi0} \cdot t < r_2 - d$ that

$$K_{fi5} > \frac{\dot{\rho}_{fi0}}{r_2 - d} \int_0^{\dot{\rho}_{fi0}} \frac{1}{b_i \eta_{fi5} \|\dot{\rho}\|_2 \dot{\rho}} d\dot{\rho} \tag{47}$$

So it can ensure that the i-th can join the cluster successfully.

In summary, follower satellites will move between no-fly zone and the communication distance of leader satellite without collision. And the external satellites could join the cluster at any time.

4. Numerical simulations and analysis

In this section, the simulation of the leader and follower layers of the distributed satellite system illustrates the effectiveness of the control method proposed in this paper. Finally, the integrated simulation of the system is given.

4.1. Synchronous control of the leader layer

Suppose that the leader layer contains 6 satellites, all of which fly around a virtual leader satellite. In order to save communication resources, a ring topology is adopted which is shown in Fig. 3.

In the figure, Vsat is the virtual leader satellite, Sat i ($i = 1, 2, ..., 6$) is the i-th satellite in leader layer, then the adjacency matrix between the satellites can be obtained as equation (41), and the initial orbit elements of the virtual leader satellite are shown in Table 1.

$$A_L = \begin{bmatrix} 0 & 1 & 0 & 0 & 0 & 1 \\ 1 & 0 & 1 & 0 & 0 & 0 \\ 0 & 1 & 0 & 1 & 0 & 0 \\ 0 & 0 & 1 & 0 & 1 & 0 \\ 0 & 0 & 0 & 1 & 0 & 1 \\ 1 & 0 & 0 & 0 & 1 & 0 \end{bmatrix} \tag{48}$$

Table 2
Initial states of the six satellites.

Satellite	Initial position (m)	Initial velocity (m/s)
1	$\rho_1(0) = [\ 1500 \quad 2000 \quad 2500\ ]^T$	$v_1(0) = [\ -1 \quad 2 \quad -3\ ]^T$
2	$\rho_2(0) = [\ -1000 \quad 3000 \quad 2000\ ]^T$	$v_2(0) = [\ -1 \quad 2 \quad 3\ ]^T$
3	$\rho_3(0) = [\ 1000 \quad -2000 \quad 3000\ ]^T$	$v_3(0) = [\ -1 \quad -2 \quad 3\ ]^T$
4	$\rho_4(0) = [\ -1000 \quad -3000 \quad 2000\ ]^T$	$v_4(0) = [\ -1 \quad 2 \quad -3\ ]^T$
5	$\rho_5(0) = [\ 1000 \quad -1500 \quad -2000\ ]^T$	$v_5(0) = [\ -2 \quad 1 \quad -3\ ]^T$
6	$\rho_6(0) = [\ -1500 \quad 3500 \quad -1000\ ]^T$	$v_6(0) = [\ -1 \quad 2 \quad -3\ ]^T$

Table 3
Desired states of the six satellites.

Satellite	Initial position (m)	Initial velocity (m/s)
1	$\rho_{1d} = [\ 0 \quad 5000 \quad 0\ ]^T$	$v_{1d} = [\ 0 \quad 0 \quad 0\ ]^T$
2	$\rho_{2d} = [\ 0 \quad 2500 \quad 2500\sqrt{3}\ ]^T$	$v_{2d} = [\ 0 \quad 0 \quad 0\ ]^T$
3	$\rho_{3d} = [\ 0 \quad -2500 \quad 2500\sqrt{3}\ ]^T$	$v_{3d} = [\ 0 \quad 0 \quad 0\ ]^T$
4	$\rho_{4d} = [\ 0 \quad -5000 \quad 0\ ]^T$	$v_{4d} = [\ 0 \quad 0 \quad 0\ ]^T$
5	$\rho_{5d} = [\ 0 \quad -2500 \quad -2500\sqrt{3}\ ]^T$	$v_{5d} = [\ 0 \quad 0 \quad 0\ ]^T$
6	$\rho_6(0) = [\ -1500 \quad 3500 \quad -1000\ ]^T$	$v_{6d} = [\ 0 \quad 0 \quad 0\ ]^T$

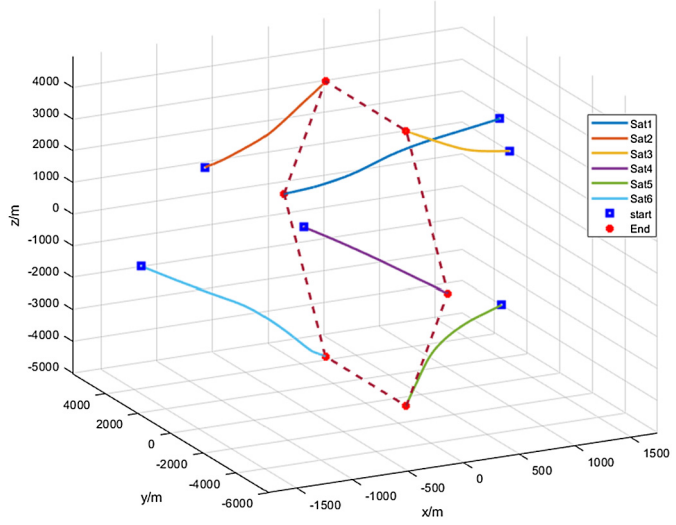

Fig. 4. Formation configuration of satellites in leader layer.

Assume that the mass of the six satellites is 50 kg and the maximum output of the thruster is 5 N. The Initial states of them in the LVLH frame are shown in Table 2, and the desired states are shown in Table 3 that can form a space regular hexagon with a side length of 5 km.

In the controller, the parameters of the FTCESO are $k_1 = 25$, $k_2 = 840$, $k_3 = 960$. The parameters of the NFTSMC are designed as $a = 0.01$, $b = 0.02$, $p = 5$, $q = 3$, $K_{i1} = 0.2$ and $K_{i2} = 0.02$. In addition, the external disturbance is the sum of J_2 perturbation and atmospheric darg which can be calculated by Eqs. (5) and (8), and the atmospheric density model CIRA1961 is cited that $\varphi_0 = 0.36$ kg/km^3, $H_0 = 37.4$ km, $\mu_0 = 0.2$ at the altitude of 200 km.

Under the action of the Synchronous controller based on FTCESO and NFTSMC, the simulation results of the satellites in leader layer can be obtained as Fig. 4, from which one can see that the satellites in the leader layer form a regular hexagon in space and maintain their configuration. The position tracking errors of satellites in leader layer are shown in Fig. 5. It can be seen from Fig. 5 that the position tracking errors of the satellites in can still quickly converge to near zero, even if the system is affected by J_2 perturbation, atmospheric drag and the thrust constraint. The convergence time is all in 620 s, and the tracking accuracy reaches 0.01 m. The control force of the satellites in the leader layer is shown in Fig. 6. It can be seen from Fig. 6 that during the control process, the amplitude of the satellite's control force is always within the range of 5 N or less. In the simulation, the controller has ideal tracking control accuracy and good coordination.

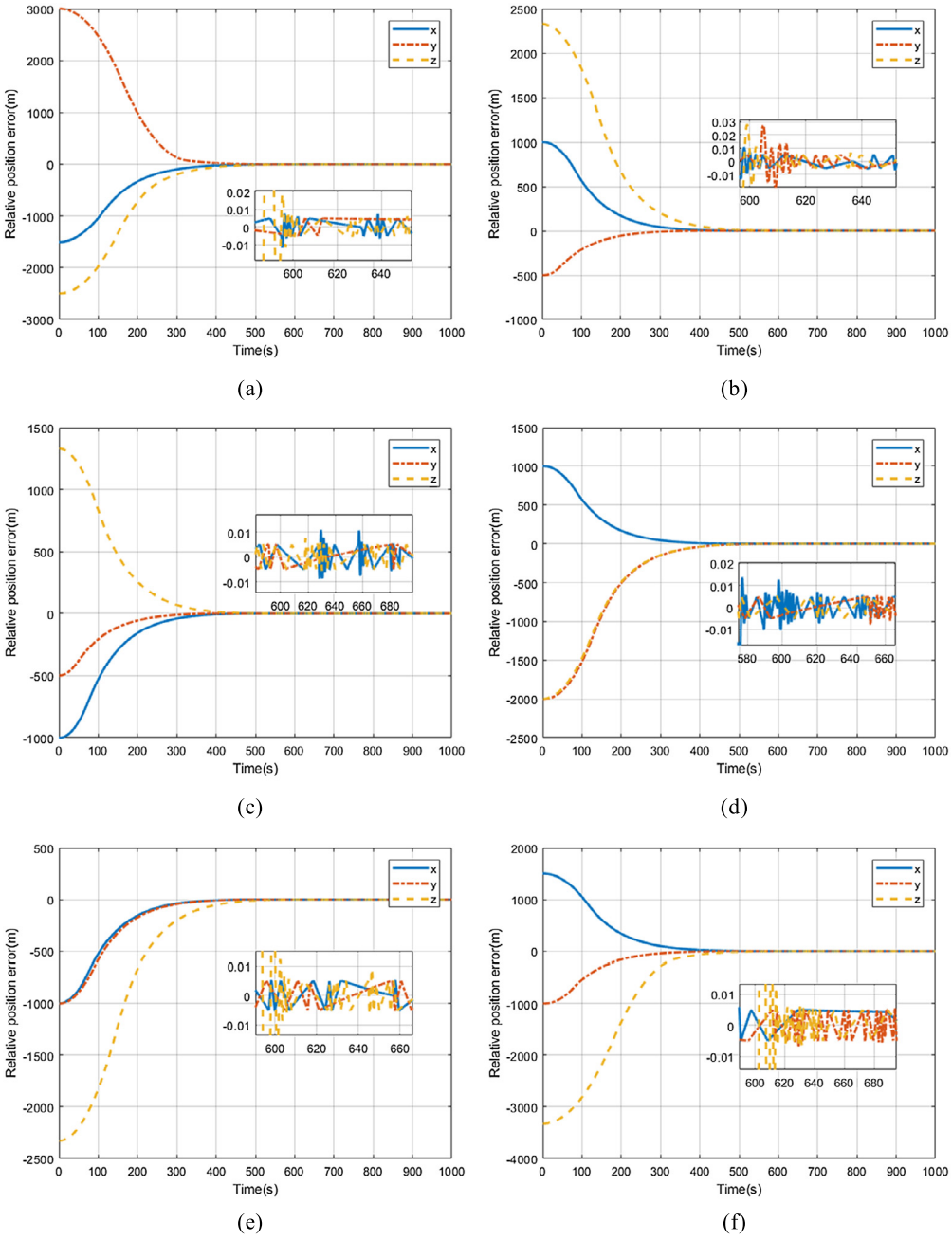

Fig. 5. Trajectories of position tracking error of the satellites in leader layer. (a) Satellite 1. (b) Satellite 2. (c) Satellite 3. (d) Satellite 4. (e) Satellite 5. (f) Satellite 6.

4.2. Collision avoidance control of the follower layer

Suppose that each satellite in the leader layer is followed by 5 satellites, and there is no communication delay between any two satellites. Taking Sat1 as an example, the 5 satellites following Sat1 are FSat*i*, (i = 1, 2,..., 5), and the topology is shown in Fig. 7. The matrix of $B_l(b_i)$ and $B_f(b_{ij})$ expressed as Eq. (49).

$$B_l = \begin{bmatrix} 1 \\ 1 \\ 1 \\ 1 \\ 1 \end{bmatrix}, \qquad B_f = \begin{bmatrix} 0 & 1 & 1 & 1 & 1 \\ 1 & 0 & 1 & 1 & 1 \\ 1 & 1 & 0 & 1 & 1 \\ 1 & 1 & 1 & 0 & 1 \\ 1 & 1 & 1 & 1 & 0 \end{bmatrix} \tag{49}$$

The mass of each satellites flying around Sat1 is 50 kg, the maximum output of the thruster is 5 N, and no space configuration is required during the entire mission.

To verify that the control method is suitable for complex space missions, it is assumed that FSat1, FSat2, and FSat3 are three satellites that have already existed around the leader satellite. FSat4 and FSat5 are two satellites that are from the space beyond the communication

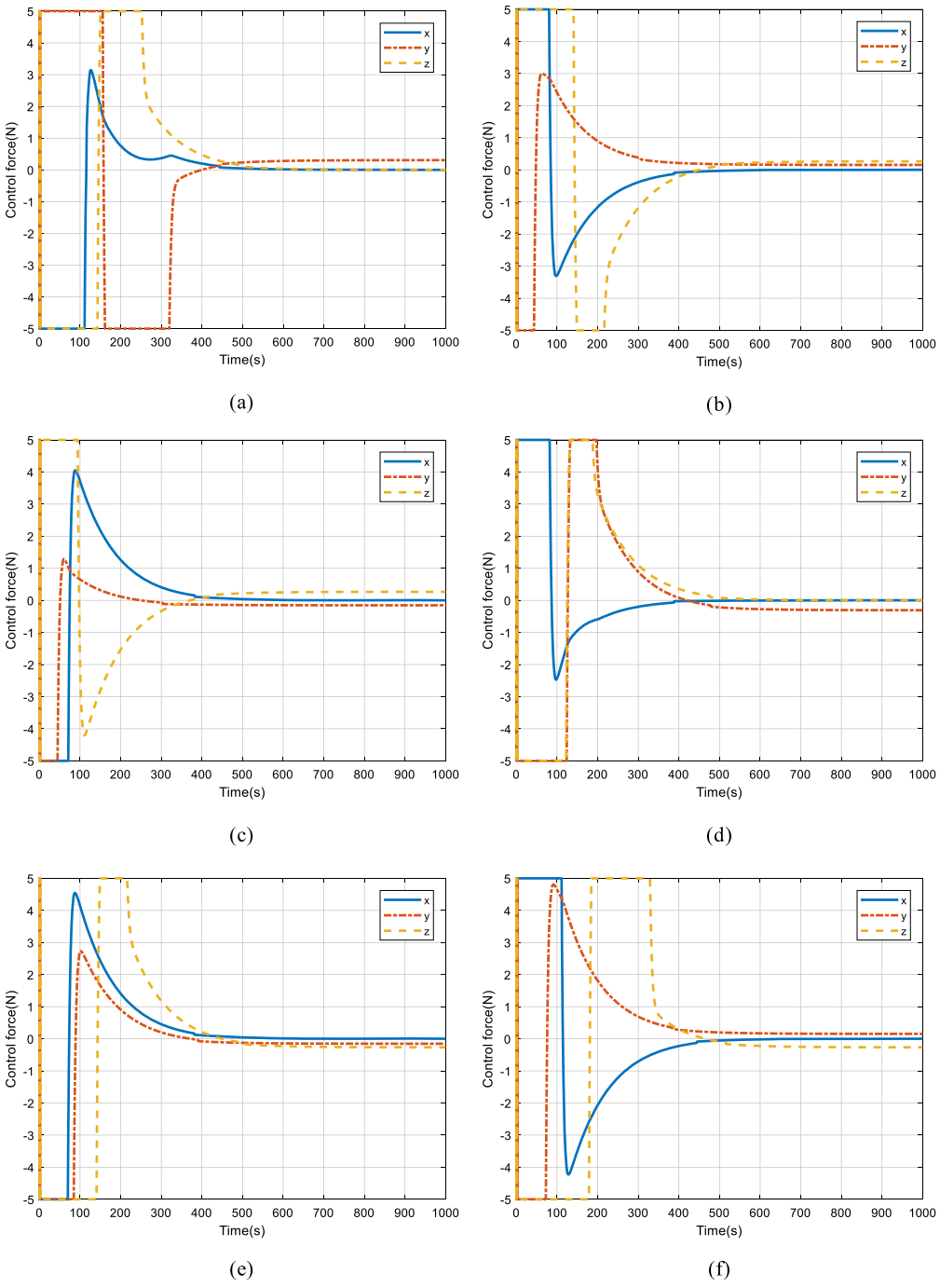

Fig. 6. The control force trajectories of the satellites in leader layer. (a) The satellite 1. (b) The satellite 2. (c) The satellite 3. (d) The satellite 4. (e) The satellite 5. (f) The satellite 6.

range and they are planed to join the cluster. In the LVLH frame of leader satellite, the initial state of the follower satellites is shown in Table 4.

Set space division parameters near the leader satellite that $d = 200$ m, $d_i = 300$ m, $r_1 = 500$ m, $r_2 = 1000$ m, $h = 1500$ m, $a_1 = 2000$ m, $a_2 = 2300$ m.

In order to verify the effectiveness of the controller, three control methods are used for comparison. The first controller is $u_1 = u_{fi1} + u_{fi2} + u_{fi3}$, the second controller is $u_2 = u_{fi1} + u_{fi2} + u_{fi3} + u_{fi4}$, and the third controller is $u_3 = u_{fi1} + u_{fi2} + u_{fi3} + u_{fi4} + u_{fi5}$. In addition, the gain coefficients of the controller are set as $K_{fi1} = 0.5$, $K_{fi2} = 0.5$, $K_{fi3} = 1000$, $K_{fi4} = 1$, $K_{fi5} = 0.2$.

The motion trajectories of FSat1, FSat2 and FSat3 under the action of the three controllers are shown in Fig. 8–Fig. 10. From Fig. 8–Fig. 10, one can see that all three controllers can keep FSat1, FSat2 and FSat3 flying within the communication range of the leader satellite. However, the initial positions of FSat1, FSat2 and FSat3 are very close in space, and the velocities in some directions are opposite. The relative distances of FSat1, FSat2 and FSat3 under the action of three controllers are shown in Fig. 11–Fig. 13. It can be seen that under the action of the controller 1, it can't always ensure that the relative distance between FSat1, FSat2 and FSat3 is beyond the safe distance, especially in the initial stage. Under the action of the controllers 2 and 3, the relative distance between FSat1, FSat2 and FSat3 can always

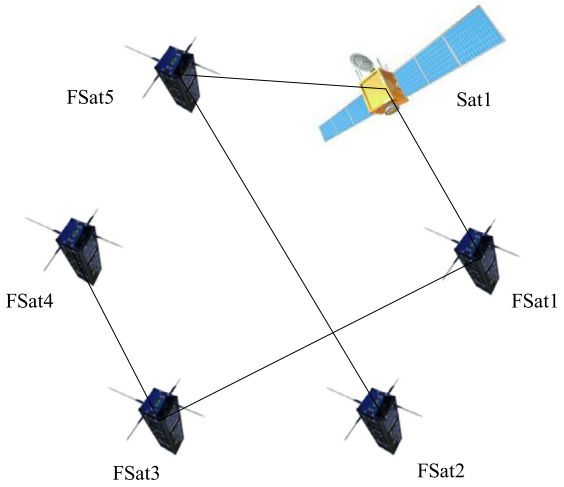

Fig. 7. Communication topology of the satellites in follower layer.

Table 4
Initial states of the follower satellites.

Satellite	Initial position (m)	Initial velocity (m/s)
1	$\rho_{f1}(0) = [\ 700 \quad -100 \quad 100\ ]^T$	$v_{f1}(0) = [\ 1 \quad 2 \quad 3\ ]^T$
2	$\rho_{f2}(0) = [\ 600 \quad 200 \quad 100\ ]^T$	$v_{f2}(0) = [\ 2 \quad -2 \quad 3\ ]^T$
3	$\rho_{f3}(0) = [\ 500 \quad -100 \quad 300\ ]^T$	$v_{f3}(0) = [\ -1 \quad -2 \quad 3\ ]^T$
4	$\rho_{f4}(0) = [\ -2500 \quad 200 \quad 400\ ]^T$	$v_{f4}(0) = [\ 3 \quad -1 \quad -2\ ]^T$
5	$\rho_{f5}(0) = [\ 2600 \quad 0 \quad 0\ ]^T$	$v_{f5}(0) = [\ -3 \quad 1 \quad -2\ ]^T$

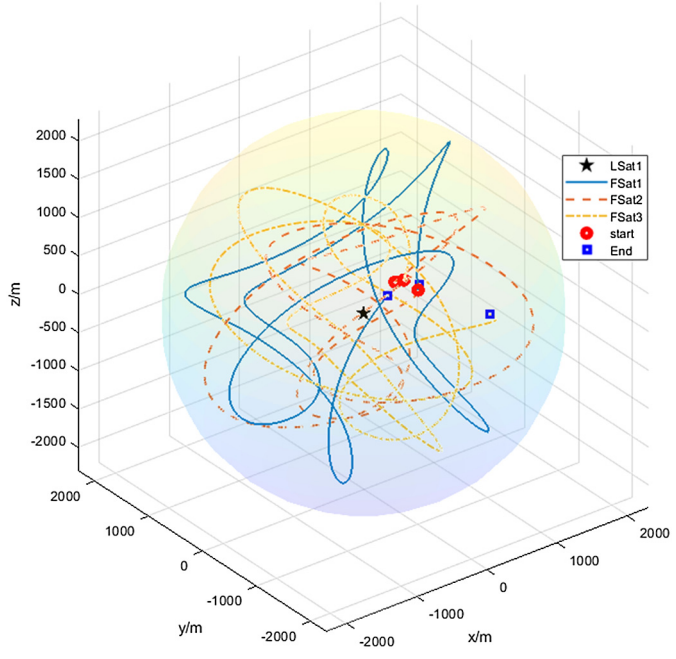

Fig. 8. Movement trajectory of FSat1, FSat2 and FSat3 under the action of controller 1.

be maintained a safe distance and completely avoid collisions between the satellites. It is worth noting that because the controller 3 includes viscous control, the relative distance between the satellites changes more smoothly than the other two controllers.

Taking FSat1 as an example, compare the control forces of the three controllers, as shown in Fig. 14–Fig. 16. In Fig. 14, only the relative distances of satellites are considered for collision avoidance in controller 1, so the control force will be great when the relative distance is too close. In addition, due to lack of timely control, the control force is greater in the whole control process, and even the output saturation occurs. As shown in Fig. 15, the controller 2 includes dynamic control of the relative velocity from the satellite, which can determine whether the satellites are flying closer to each other in advance. The control force is only half of the controller 1, and the controller 2 is rarely saturated. Since the controller 3 includes viscous control, the velocities of the satellites are all reduced, so that the control force can be greatly reduced, as shown in Fig. 16.

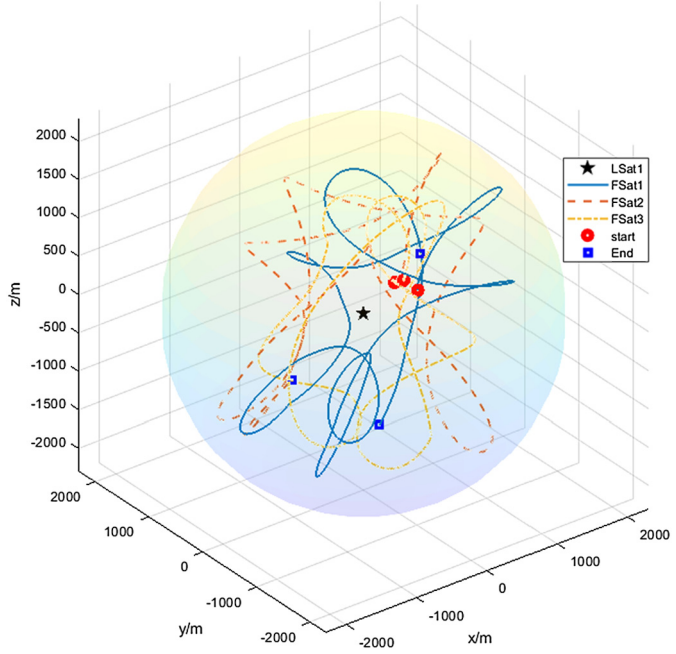

Fig. 9. Movement trajectory of FSat1, FSat2 and FSat3 under the action of controller 2.

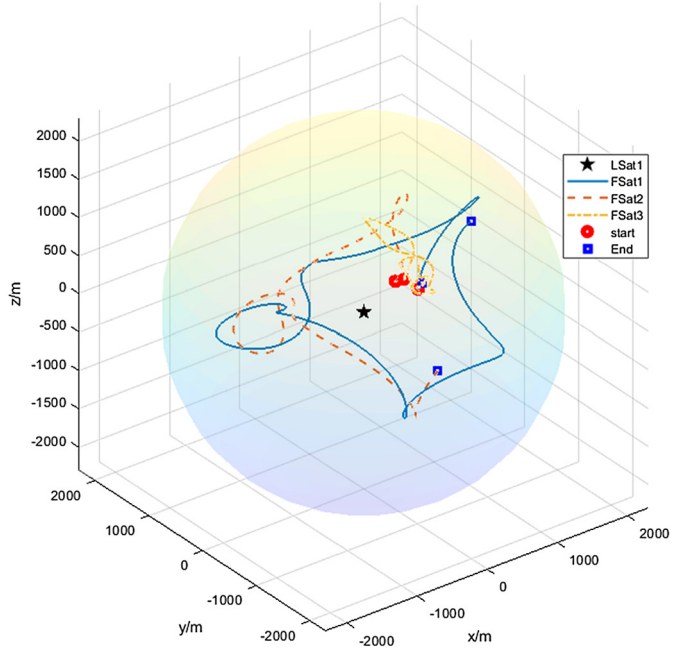

Fig. 10. Movement trajectory of FSat1, FSat2 and FSat3 under the action of controller 3.

The movement trajectories under the action of three controllers are shown in Fig. 17–Fig. 19, and the relative distance between FSat4, FSat5 and the leader satellite under the action of controller 3 are shown in Fig. 20. As shown in Fig. 17 and Fig. 18, since the artificial potential fields in controllers 1 and 2 are symmetrical and do not contain viscous control terms, it is less possible to control the satellite from outside into the cluster. But for the controller 3 that contains viscous control, the velocity of the external satellite has been decreasing after flying into the cluster, and it can keep flying within the communication distance of the leader satellite, and then complete the operation of joining the cluster.

Conclusions

This paper proposes a hierarchical control strategy that includes both formation flying and satellite cluster for distributed satellite system. The satellites that need a specific space configuration and the rest of the satellites in the satellite system are divided into leader layer and follower layer. The synchronization control based on FTCESO and NFTSMC is designed for the leader layer, and its stability is proved to ensure that the satellites in leader layer can stabilize to the desired position in a limited time under the conditions of multiple disturbances and thrust constraints. For follower layer, an cluster collision avoidance controller based on improved artificial potential field

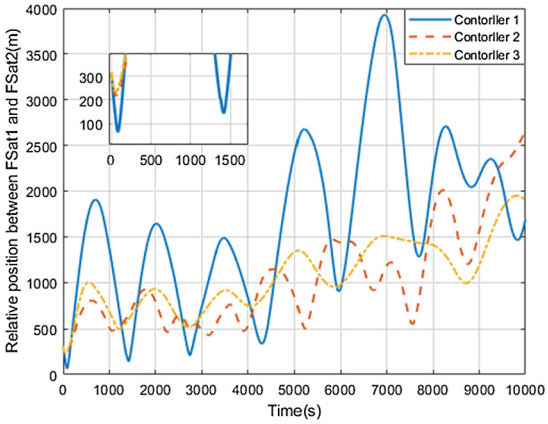

Fig. 11. Relative distance between FSat1 and FSat2.

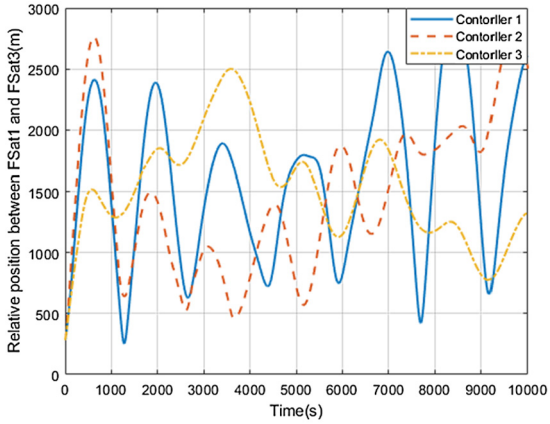

Fig. 12. Relative distance between FSat1 and FSat3.

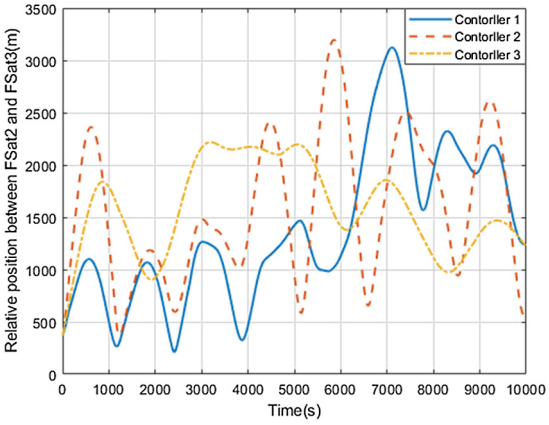

Fig. 13. Relative distance between FSat2 and FSat3.

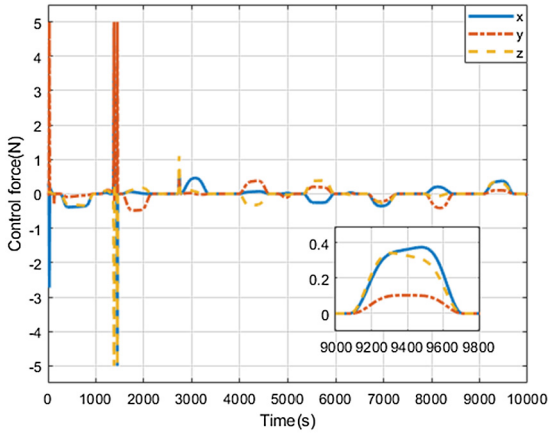

Fig. 14. FSat1 control force under the action of controller 1.

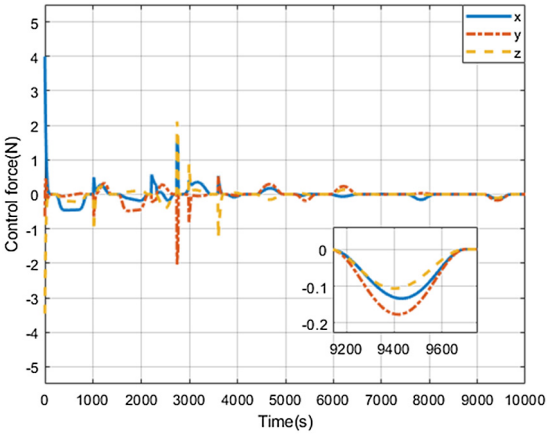

Fig. 15. FSat1 control force under the action of controller 2.

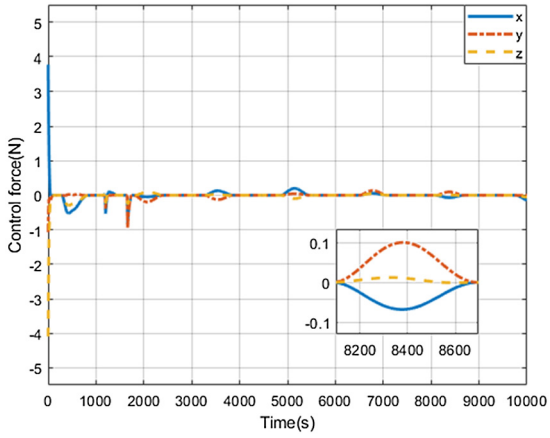

Fig. 16. FSat1 control force under the action of controller 3.

method is designed, which includes dynamic avoidance and viscous control. It can not only ensure that the satellite follows leader satellite in the communication range without collision, but also can absorb the external satellite into the follower layer to form a new cluster.

Declaration of competing interest

The authors declare that they have no known competing financial interests or personal relationships that could have appeared to influence the work reported in this paper.

Acknowledgements

This work is supported by Natural Science Foundation of Shaanxi Province (2020JQ-132), China Postdoctoral Science Foundation (2020M683571) and the Fundamental Research Funds for the Central Universities (3102019HTQD007).

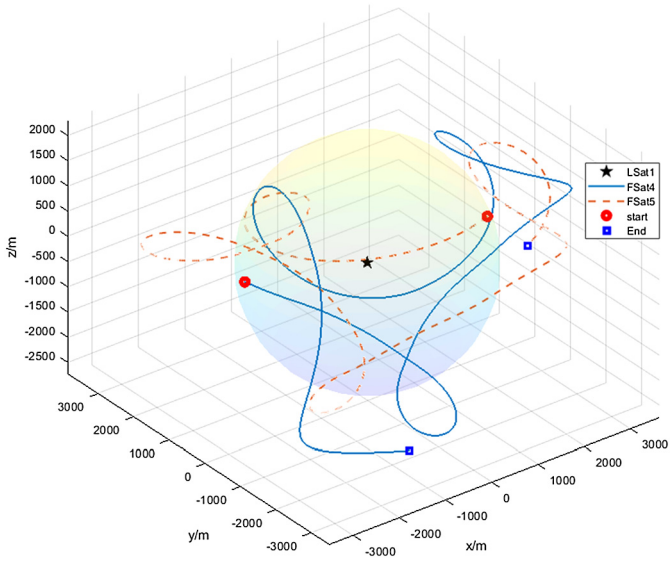

Fig. 17. Movement trajectory of FSat4 and FSat5 under the action of controller 1.

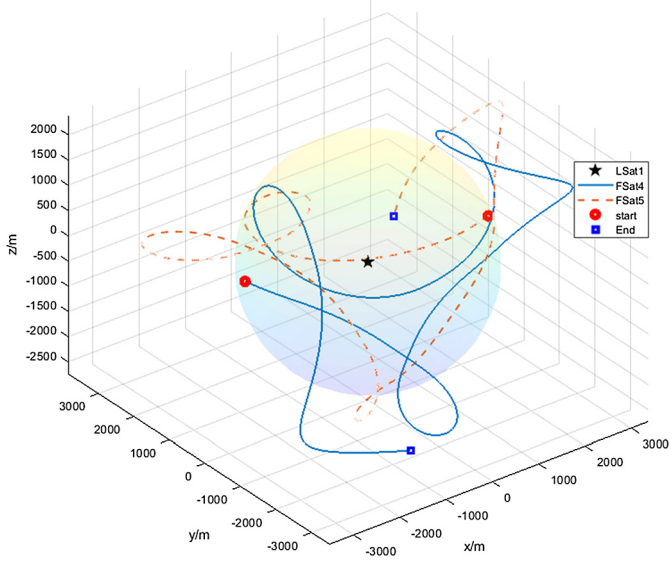

Fig. 18. Movement trajectory of FSat4 and FSat5 under the action of controller 2.

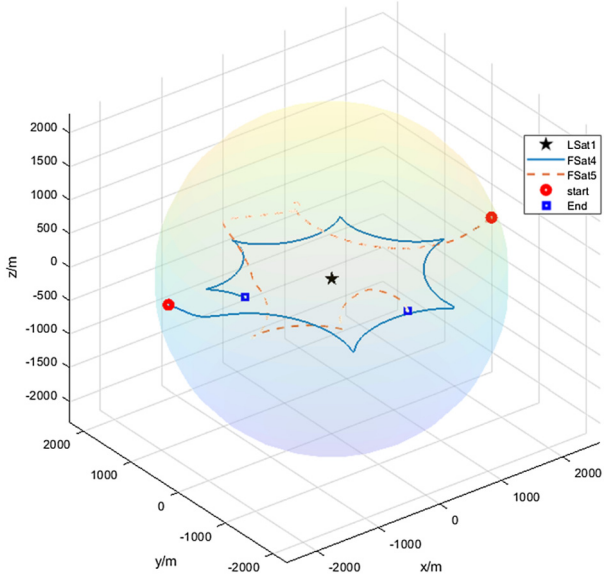

Fig. 19. Movement trajectory of FSat4 and FSat5 under the action of controller 3.

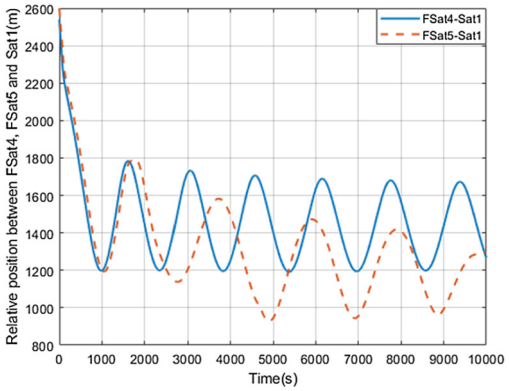

Fig. 20. The relative distance between FSat4, FSat5 and the leader satellite under the action of controller 3.

References

[1] Harish M. Manohara, et al., On development of 100-gram-class spacecraft for swarm applications, IEEE Syst. J. 10 (2) (2016) 673–684.

[2] C. Liu, D. Ye, K. Shi, Z. Sun, Robust high-precision attitude control for flexible spacecraft with improved mixed H_2/H_∞ control strategy under poles assignment constraint, Acta Astronaut. 136 (2017) 166–175.
[3] C. Liu, K. Shi, Z. Sun, Robust H_∞ controller design for attitude stabilization of flexible spacecraft with input constraints, Adv. Space Res. 63 (5) (2019) 1498–1522.
[4] T. Chen, H. Wen, Z. Wei, Distributed attitude tracking for multiple flexible spacecraft described by partial differential equations, Acta Astronaut. 159 (2019) 637–645.
[5] X. Ren, K. Zhang, X. Li, et al., Precise point positioning with multi-constellation satellite systems: BeiDou, Galileo, GLONASS, GPS, Acta Geod. Cartographica Sin. 44 (12) (2015) 1307.
[6] R. Kristiansen, P.J. Nicklasson, Spacecraft formation flying: a review and new results on state feedback control, Acta Astronaut. 65 (11–12) (2009) 1537–1552.
[7] L. Mazal, P. Gurfil, Closed-loop distance-keeping for long-term satellite cluster flight, Acta Astronaut. 94 (1) (2014) 73–82.
[8] C. Liu, Z. Sun, K. Shi, F. Wang, Robust dynamic output feedback control for attitude stabilization of spacecraft with nonlinear perturbations, Aerosp. Sci. Technol. 64 (2017) 102–121.
[9] K. Shi, C. Liu, Z. Sun, et al., Disturbance observer-based attitude stabilization for rigid spacecraft with input MRCs, Adv. Space Res. 66 (3) (2020) 689–701.
[10] M. Ran, Q. Wang, C. Dong, Stabilization of a class of nonlinear systems with actuator saturation via active disturbance rejection control, Automatica 63 (2016) 302–310.
[11] M. Ran, Q. Wang, C. Dong, Active disturbance rejection control for uncertain nonaffine-in-control nonlinear systems, IEEE Trans. Autom. Control 62 (11) (2016) 5830–5836.
[12] D.J. Zhao, D.G. Yang, Model-free control of quad-rotor vehicle via finite-time convergent extended state observer, Int. J. Control. Autom. Syst. 14 (1) (2016) 242–254.
[13] Z. Cai, J. Lou, J. Zhao, et al., Quadrotor trajectory tracking and obstacle avoidance by chaotic grey wolf optimization-based active disturbance rejection control, Mech. Syst. Signal Process. 128 (Aug. 1, 2019) 636–654.
[14] J. Li, Y. Pan, K.D. Kumar, Design of asymptotic second-order sliding mode control for satellite formation flying, J. Guid. Control Dyn. 35 (1) (2012) 309–316.
[15] C. Liu, X. Yue, K. Shi, Z. Sun, Inertia-free attitude stabilization for flexible spacecraft with active vibration suppression, Int. J. Robust Nonlinear Control 29 (18) (2019) 6311–6336.
[16] H. Du, S. Li, C. Qian, Decentralized sliding-mode control for attitude synchronization in spacecraft formation, Int. J. Robust Nonlinear Control 23 (11) (2012) 1183–1197.
[17] L. Xing, J. Zhang, C. Liu, et al., Fuzzy-logic-based adaptive event-triggered sliding mode control for spacecraft attitude tracking, Aerosp. Sci. Technol. 108 (2021) 106394.
[18] A.M. Zou, K.D. Kumar, Z.G. Hou, et al., Finite-time attitude tracking control for spacecraft using terminal sliding mode and Chebyshev neural network, IEEE Trans. Syst. Man Cybern., Part B, Cybern. 41 (4) (2011) 950–963.
[19] Y. Feng, X. Yu, Z. Man, Non-singular terminal sliding mode control of rigid manipulators, Automatica 38 (12) (2002) 2159–2167.
[20] T. Chen, J. Shan, Rotation-matrix-based attitude tracking for multiple flexible spacecraft with actuator faults, J. Guid. Control Dyn. 42 (1) (2019) 181–188.
[21] X. Bao, D. Wang, Nonsingular fast terminal sliding mode control for spinning missiles based on extended state observer, Int. J. Pattern Recognit. Artif. Intell. 33 (01) (2019) 1959001.
[22] H. Gui, G. Vukovich, Adaptive fault tolerant spacecraft attitude control using a novel integral terminal sliding mode, Int. J. Robust Nonlinear Control 27 (16) (2017) 3174–3196.
[23] H. Zhang, P. Gurfil, Nanosatellite cluster keeping under thrust uncertainties, J. Guid. Control Dyn. 37 (5) (2014) 1406–1414.
[24] L. Mazal, G. Mingotti, P. Gurfil, Optimal on-off cooperative manoeuvers for long-term satellite cluster flight, J. Guid. Control Dyn. 37 (2) (2014) 391–402.
[25] F.G. Zimmerman, P. Gurfil, Optimal target states for satellite cluster flight control on near-circular orbits, J. Guid. Control Dyn. 38 (3) (2015) 375–383.
[26] C. Wen, H. Zhang, P. Gurfil, Orbit injection considerations for cluster flight of nanosatellites, J. Spacecr. Rockets 52 (1) (2015) 196–208.
[27] H. Zhang, P. Gurfil, Satellite cluster flight using on-off cyclic control, Acta Astronaut. 106 (2015) 1–12.
[28] H. Zhang, P. Gurfil, Distributed control for satellite cluster flight under different communication topologies, J. Guid. Control Dyn. (2015) 1–11.
[29] C. Liu, K. Shi, X. Yue, et al., Inertia-free saturated output feedback attitude stabilization for uncertain spacecraft, Int. J. Robust Nonlinear Control 30 (13) (2020) 5101–5121.
[30] O. Khatib, Real-time obstacle avoidance for manipulators and mobile robots, in: Proceedings. 1985 IEEE International Conference on Robotics and Automation, IEEE, 1985.
[31] K. Shi, C. Liu, J.D. Biggs, et al., Observer-based control for spacecraft electromagnetic docking, Aerosp. Sci. Technol. 99 (2020) 105759.
[32] K. Shi, C. Liu, Z. Sun, Constrained fuel-free control for spacecraft electromagnetic docking in elliptical orbits, Acta Astronaut. 162 (2019) 14–24.